Plasma Sources Science and Technology

PAPER

# Charge transfer from doubly charged ions of transition elements in a neon glow discharge: evidence based on emission spectra

To cite this article: Zdenk Weiss and Juliet C Pickering 2020 *Plasma Sources Sci. Technol.* **29** 045025



IOP Publishing Plasma Sources Science and Technology
Plasma Sources Sci. Technol. **29** (2020) 045025 (12pp) https://doi.org/10.1088/1361-6595/ab82b2

# Charge transfer from doubly charged ions of transition elements in a neon glow discharge: evidence based on emission spectra

**Zdeněk Weiss**[1,3] **and Juliet C Pickering**[2]

[1] Institute of Physics of the Czech Academy of Sciences, Na Slovance 2, 182 21 Praha 8, Czech Republic
[2] Blackett Laboratory, Imperial College London, Prince Consort Road, London, SW7 2AZ, United Kingdom

E-mail: weissz@fzu.cz

Received 10 July 2019, revised 13 March 2020
Accepted for publication 24 March 2020
Published 22 April 2020

**Abstract**

An extensive study of Mn II, Fe II, Ti II, Cr II and Cu II emission spectra from a Grimm-type glow discharge in neon was performed, using the formalism of transition rate (TR) diagrams. In this method, radiative depopulation rates of individual excited levels of a species under study are established based on the emission spectrum, prospective contributions from radiative decay of higher excited levels (cascade excitation) are subtracted and the resulting net depopulation rates are plotted as function of energy of the levels involved. A peak at a particular energy in such a diagram reflects a collisional process in operation, selectively populating levels in a narrow interval around that energy. By comparing net TR diagrams of ionic spectra of the elements listed above, a common pattern was found indicating that singly charged ions of these elements are created, in addition to other mechanisms, by charge transfer between doubly charged ions of the element under study and metastable neutral neon atoms. This mechanism appears to be significant and needs to be taken into account in collisional–radiative models describing excitation and ionization of some elements in neon glow discharges.

Keywords: glow discharge, emission spectroscopy, doubly charged ions, charge transfer, transition rate diagrams

## 1. Introduction

Emission spectroscopy of laboratory plasmas is an extensive discipline with applications in various fields, involving analytical chemistry [1, 2], the diagnostics and optimization of plasma deposition processes [3], the measurements of fundamental atomic data for astrophysics [4], hollow cathode metal ion lasers [5] and many other areas of plasma science and technology. Many common methods of plasma diagnostics by optical spectroscopy rely on the concept of local thermodynamic equilibrium (LTE) [3, 6, 7] and the interpretation of emission spectra proceeds in terms of excitation- and ionization temperatures, assuming the Saha–Boltzmann distribution of the excited and ionized species present. Glow discharges (GD), however, are weakly ionized plasmas, of a non-equilibrium nature, for which this approach does not work. Therefore they must be treated differently, by collisional–radiative models, taking into account all major elementary processes responsible for the excitation and ionization of the species of interest. Emission spectroscopy contributes to this effort by testing the predictions of the modelling and identifying the most significant processes that need to be accounted for. In laboratory plasmas, major excitation and ionization processes are the electron- and heavy particle collisions. An

[3] Author to whom any correspondence should be addressed.

 

important class of the latter are the charge transfer (CT) reactions [8], first described in 1929 by Duffendack and Black [9]. In 1987, Steers and Fielding proved that the excitation of the 224.7 nm Cu II line, one of the strongest Cu lines emitted by a glow discharge in argon with a copper cathode, is caused by a CT reaction between argon metastable ions (Ar II, $3s^2 3p^5\ ^2P^\circ_{1/2}$) and neutral copper atoms [10]. This was a major step towards understanding how analytical glow discharges work. In numerous further studies listed in [11], Steers and his colleagues measured GD emission spectra of many elements at different conditions, e.g., with different discharge gases, and plotted intensity ratios of the emission lines observed as functions of their excitation energy. Thereby they were able to identify some selective reactions, such as CT, in which relative excitation cross sections for individual states accessible to these reactions peak in the close vicinity of a certain resonant energy. In 2014, Weiss *et al* substantially improved this method by introducing the concept of transition rate (TR) diagrams [12], a formalism suitable for the analysis of emission spectra of plasmas in which radiative decay rates of excited states dominate over the rates of their collisional depopulation by electrons, and applied this formalism to GD spectra of singly charged ions of certain transition elements. Through TR diagrams it is possible to track the decay paths of excited states, based on an emission spectrum covering a sufficiently wide wavelength range. In 2009 and 2010, the authors of paper [12] collected high-resolution GD emission spectra of a number of elements using the high resolution VUV–VIS Fourier transform spectrometer at Imperial College, London, United Kingdom. The data from those campaigns still continues to be analyzed and here we report results based on the spectra of Mn, Fe, Ti, Cr and Cu in a neon discharge. More specifically, it was clearly demonstrated [12–14] that the second (ionic) GD emission spectra of the elements studied so far are dominated by heavy particle collisional excitation and cascading, with selective excitation of certain levels, depending on the electronic structure of the species involved. By comparing the GD excitation of different elements, it is possible to identify similarities that can be attributed to a common excitation mechanism. In this paper such comparisons are made between Cr II, Fe II, Ti II, Cu II and Mn II spectra in a neon glow discharge, resulting in evidence that charge transfer from doubly charged ions of these elements to neon metastable atoms takes place. To our knowledge, this is the first report of this mechanism to play a role in a glow discharge.

## 2. Experimental

The emission spectra discussed in this paper were all obtained from the Grimm-type GD source, a spectral source widely used in analytical chemistry as the basis of glow discharge optical emission spectroscopy (GD-OES) [15, 16]. It is a simple device consisting of a flat cathode (the sample) and a perpendicularly oriented tubular anode, separated from the cathode by a narrow gap, see figure 1. Glow discharge in a noble gas at a pressure of several hPa runs between these two electrodes and is constricted in the space inside the anode cavity, by keeping the inter-electrode distance small enough to prevent the

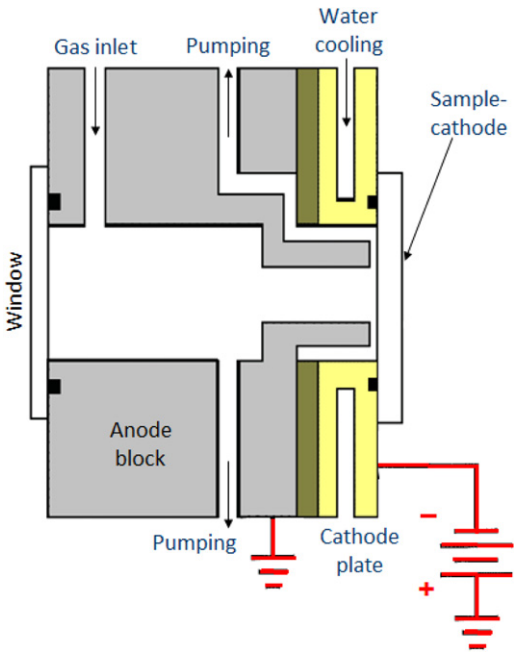


**Figure 1.** The Grimm-type glow discharge source.

discharge from spreading to the gap between the anode wall and the cathode (the Paschen breakdown law [15]). The source is operated in a regime of abnormal glow discharge [15], so that the cathode is sputtered and the sputtered atoms and ions of the cathode material enter the negative glow region, are excited and emit radiation. The spectrum is observed end-on, through a $MgF_2$ window, in the axial direction. The transport of the sputtered and thermalized sample material in the discharge cell proceeds by diffusion and can be described as a 2D-problem within the anode cavity, with a cylindrical symmetry and boundary conditions at the cathode (the input flux) and the anode wall where this material settles (redeposition). The window is far enough from the cathode so that no problem with its transmittance due to redeposition occurred throughout the experiments. Internal anode diameter was 4.0 mm. The samples studied (cathode materials) were pure metals Mn, Fe, Ti, Cr and Cu (purity $> 99.5\%$ of the element or better). The discharge was operated at constant voltage and constant current at 700 V, 20 mA, in pure neon and pure argon of the 5.0 purity (99.999%), at a pressure adjusted so that the electrical parameters mentioned above were kept for the given cathode and the given discharge gas.

The spectra were recorded using the high resolution VUV-VIS Fourier transform spectrometer (FTS) at Imperial College [17]. The goal was to collect intensity calibrated spectra over a wide wavelength range, so that virtually all major radiative deexcitation paths of the species under study are represented and the resulting TR diagrams are as complete as possible. A high resolving power is necessary, as typical GD spectra of transition elements consist of hundreds of lines that need to be resolved and unambiguously identified. Three wavelength ranges were selected by choosing appropriate free spectral ranges and suitable photomultiplier tube detectors and, where needed, optical filters. The combined wavelength range of these FTS measurements was from 160–600 nm.

**Table 1.** Summary of the spectral data used.

| Element | The number of lines observed (Ne discharge, 151–630 nm) Me I | Me II | Me III | The number of levels in the Me II TR diagram | References: Identification of Me II lines | References: Me II TR diagram |
|---|---|---|---|---|---|---|
| Fe | 376 | 1501 | | 519 | [27, 28] | [12, 14, 26] |
| Mn | 220 | 345 | | 149 | [25] | [12, 18] |
| Cu | 117 | 196 | | 84 | [29] | [12, 20] |
| Ti | 383 | 596 | 15 | 198 | [22–24] | [13] |
| Cr | 243 | 1431 | | 574 | [30] | [38] |

Resolution used was: 0.035 $cm^{-1}$ for the visible region (>365 nm); 0.05 $cm^{-1}$ for the intermediate region (250–365 nm), and 0.07 $cm^{-1}$ for the UV–VUV region (151–250 nm). This corresponds to a resolution of 0.28 pm at 200 nm. To obtain accurate relative line intensities, the areas under the line profiles were integrated. In the case of very significant hyperfine splitting, the individual hyperfine components were integrated, so that all hyperfine components were included. Radiometric calibration of the instrument, providing its spectral response as a function of the wavelength, was performed using standard lamps, a tungsten–halogen lamp and a deuterium lamp, with known spectral radiance, and by the branching ratio method [6] with different Fe I, Fe II and Ar I line pairs. Sets of spectra were recorded over the course of ≈2–3 h so that any effect of variation in spectral response of the FTS with time would be negligible. More details can be found in our earlier papers concerning the spectra of individual elements [13, 14, 18, 20].

Individual lines in the spectra were identified largely according to the NIST atomic spectra database [19] and some earlier versions thereof, and the original atomic data sources are listed separately for each element in table 1, together with a summary of the spectral information used. In this table and throughout the paper, 'Me' is a symbol for any of the elements listed. In columns 2–4 are the numbers of identified lines observed in the FTS spectra and used in the analysis. Column 5 gives the numbers of levels actually included in the TR diagrams. TR diagrams of Me II spectra of the elements listed here were presented for each element separately in our earlier publications, also listed in the last column of table 1.

## 3. Results and discussion

The results presented here concern the second (ionic) spectra of iron, manganese, copper, titanium and chromium. As a starting point, we discuss TR diagrams of Fe II in an argon and a neon GD (figures 2 and 3). The relative intensity $I_{ij}$ of an emission line associated with a radiative transition between an upper level $i$ and a lower level $j$ of an atom or ion can be given by:

$$I_{ij} = r_{ij}E_{ij} = r_{ij}\frac{hc}{\lambda_{ij}} \qquad (1)$$

where $\lambda_{ij}$ is the wavelength of this line, $E_{ij}$ is the energy difference between the levels $i$ and $j$, $r_{ij}$ is the rate of this transition, i.e., the number of quanta of wavelength $\lambda_{ij}$ emitted

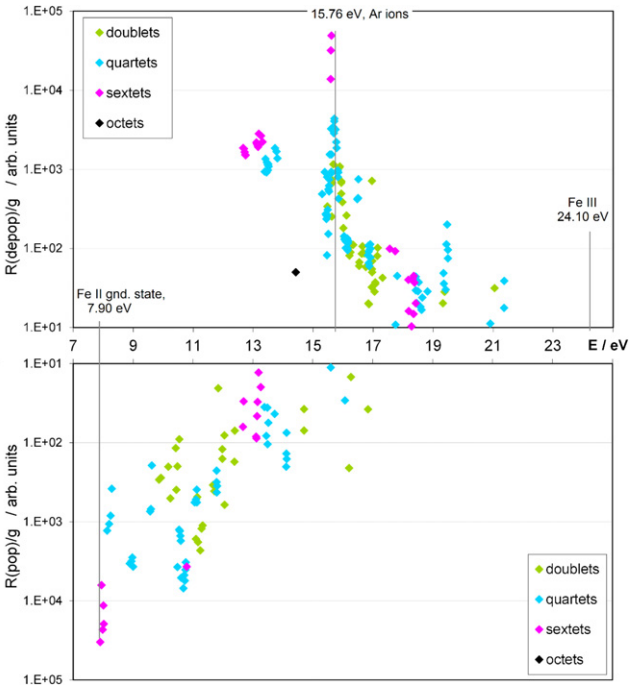


**Figure 2.** Fe II TR diagram in an argon glow discharge. Reproduced from Ref. [26] with permission of Elsevier B. V.

per second. Hence, the rate $r_{ij}$ is proportional to the product $I_{ij}\lambda_{ij}$ and transition rates associated with different emission lines can be evaluated from the observed spectrum, except for a common multiplicative constant. Each level $i$ is radiatively *depopulated* at a rate $R_i^{\text{depop}}$ equal to the sum of the rates of all transitions associated with the lines of which $i$ is the upper level, and a level $j$ is radiatively *populated* at a rate $R_j^{\text{pop}}$ equal to the sum of the rates of the radiative transitions populating this level, i.e., those transitions for which $j$ is the lower level:

$$R_i^{\text{depop}} = \sum_{k<i} r_{ik}; \quad R_j^{\text{pop}} = \sum_{k>j} r_{kj} \qquad (2)$$

A TR diagram consists of two plots with a common abscissa scale: in the upper plot, radiative *depopulation* rates ($R^{\text{depop}}$) of individual levels are plotted as functions of the level energy, and in the lower plot, the same is done with radiative *population* rates ($R^{\text{pop}}$), except that the ordinate scale in the lower plot has values increasing downward. Energies of the levels are given relative to the ground state of the *atom* throughout this paper, unless specified otherwise.

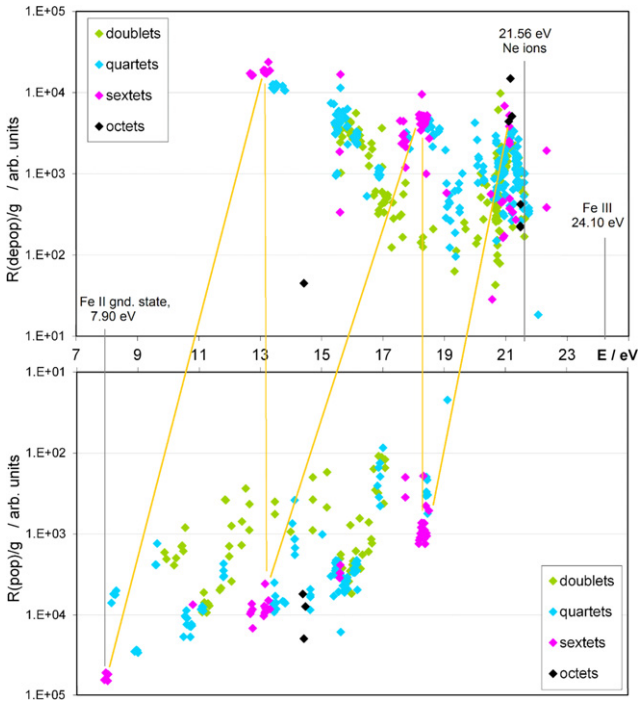


**Figure 3.** Fe II TR diagram in a neon glow discharge. Reproduced from Ref. [26] with permission of Elsevier B. V.

If the lifetime of the upper state of an emission line is largely limited by radiative decay, then the rate of collisional excitation of this state will be equal to its *net depopulation rate*, $R^{\text{net}}$, i.e., the difference between the rate of its radiative de-excitation and the rate of its radiative excitation:

$$R_i^{\text{net}} = R_i^{\text{depop}} - R_i^{\text{pop}} \tag{3}$$

Hence, a peak in the upper plot of a TR diagram, not balanced by a peak corresponding to the same levels in the lower plot, indicates that a collisional process is in operation, which selectively populates levels having energies in the position of the peak. To be able to compare the relative probabilities of individual levels being populated/depopulated, transition rates divided by the statistical weight (degeneracy factor) $g$ of the respective level are plotted, as seen in figures 2 and 3.

As recognized earlier [12], the Fe II emission spectrum in an Ar glow discharge is dominated by radiative decay of Fe II states excited by asymmetric CT between $Ar^+$ ions and neutral Fe atoms:

$$Fe^0 + Ar^+ \rightarrow Fe^{+*} + Ar^0 + \Delta E \tag{4}$$

In the TR diagram of Fe II in figure 2, this reaction is responsible for a major peak of the Fe II depopulation rate just below the argon ionization energy, 15.76 eV (the $y^6P^\circ$–$a^6D$ multiplet, with upper levels at 15.59–15.61 eV)[4]. In a neon discharge (figure 3), the situation is more complex: asymmetric CT from $Ne^+$ ions,

$$Fe^0 + Ne^+ \rightarrow Fe^{+*} + Ne^0 + \Delta E \tag{5}$$

[4] Throughout this paper, energies of ionic levels are relative to the ground state of the *atom*, i.e.energy of a Fe II level is its energy relative to the Fe II ground state + the Fe ionization energy (7.9025 eV).

is still a major source of excited $Fe^+$ ions, see the peak of Fe II depopulation rate slightly above 21.0 eV, close to the neon ionization energy (21.56 eV), in the TR diagram in figure 3. But, unlike the discharge in argon, there is a massive cascade de-excitation via a chain of lower Fe II levels. In figure 3, this cascade is marked for the sextet system by oblique yellow lines. Another difference is that, whilst the $Ar^+$–$Fe^0$ CT reaction, equation (4), preserves total spin[5] (the Wigner spin rule [6, 8]), in the case of the $Ne^+$–$Fe^0$ CT reaction, equation (5), besides the expected sextets and quartets, high depopulation rates were observed also from octet Fe II states around the resonance energy. The Wigner spin rule thus does not hold[6]. To reveal further possible selective excitation channels of iron ions in a neon discharge, a further step must be taken in the analysis of their emission spectrum. An obvious possibility is to calculate *net radiative depopulation rates* for the Fe II states the emission from which was observed, by subtracting their cascade excitation rates from the observed depopulation rates (equation (3)), and plot the resulting net rates as a function of excitation energy. More specifically, a possible quantity to be plotted is the total net radiative depopulation rate of all Fe II levels falling within a certain energy interval, irrespective of their multiplicity, with the individual energy intervals in such plot being of equal width. Unlike TR diagrams shown in figures 2 and 3, the goal here is not to display relative *probability* of a radiative decay of a specific level but relative *rate per unit of excitation energy*. Thus it is possible to allow for the effect of a variable density of excited Fe II states in different energy regions in the resulting plot. The energy step (the unit energy interval) for such a plot should be comparable with the characteristic resonance width, typical for selective excitation processes of this type. Charge transfer reactions at thermal energies such as those given by equation (2) and (3) have the largest rates for levels of the product ion lying some 0.1–0.4 eV below the combined internal energy of the reacting species [8]. Therefore, the net transition rates are plotted here with energy steps of 0.2 eV. The net-TR diagram of Fe II in a neon discharge is shown in figure 4. The most prominent peak just below the ionization energy of neon (21.56 eV) is attributed to the $Ne^+$–$Fe^0$ CT reaction, equation (5). Also indicated in this diagram is the energy of neon metastables, Ne I, $^2[^3/_2]^\circ_2$, 16.62 eV. Fe II states below this energy can be populated by Penning ionization (PI) of neutral iron atoms by neon metastables:

$$Fe^0 + Ne^0{}_M \rightarrow Fe^{+*} + Ne^0{}_0 + e^- \tag{6}$$

[5] The ground state of neutral iron is a quintet, hence, the excited iron ions produced by reaction (4) may be quartets and sextets, in conformance with the observation (see figure 2).

[6] Spin multiplicity, $2S + 1$, where $S$ is the spin angular momentum, is preserved in electric dipole transitions, hence, most spectral lines are associated with transitions between levels with the same multiplicity. For transition group elements, there are transitions from higher lying levels not preserving multiplicity, because of level mixing. If there is deviation from pure $LS$ coupling, terms may contain admixtures of different $L$ and $S$ angular momenta. Then, if terms are designated by their dominant $LS$ components, the $\Delta S = 0$ selection rule may appear to break down because of transitions occurring through non-dominant components [6].

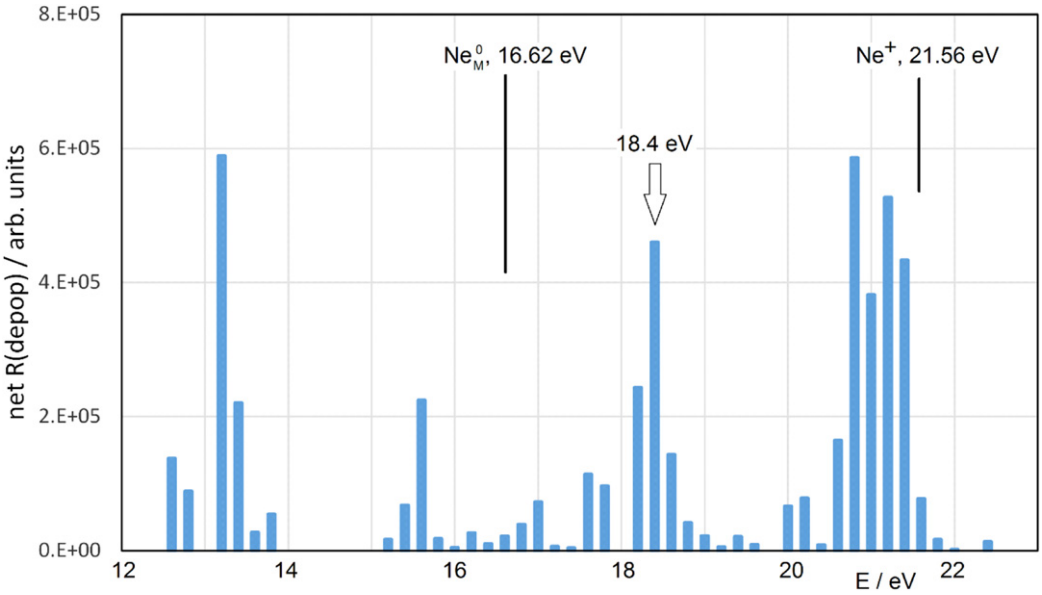


**Figure 4.** Net radiative depopulation rate of Fe II excited states as function of their energy in a neon GD.

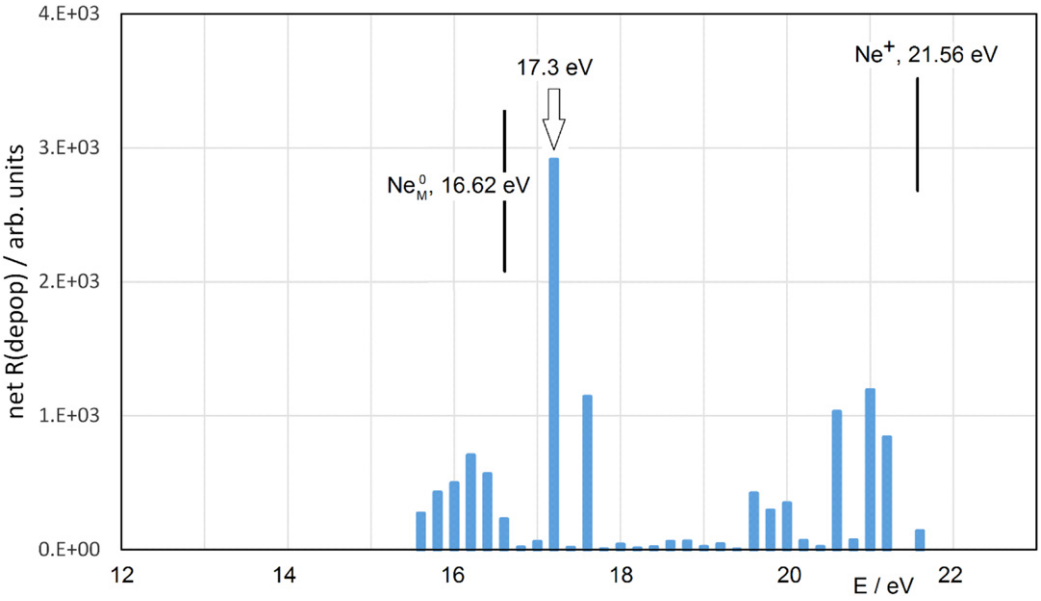


**Figure 5.** Net radiative depopulation rate of Mn II excited states as function of their energy in a neon GD.

Unlike CT, Penning ionization does not have a resonance character [6] because the electron released can carry the excess energy away. The distribution of PI-excited Fe II levels and the corresponding excitation rates depend on the electronic structure of the $Fe^+$ ion below 16.62 eV. Also, the high Fe II radiative depopulation rates around 13 eV may be caused by electron impact (EI) excitation of ground state- or metastable $Fe^+$ ions [14]. But there is a prominent peak at ≈18.4 eV of the Fe II radiative depopulation rate, marked by an arrow in figure 4, that cannot be explained by either of these mechanisms. A similar situation exists in the net-TR diagram of manganese ions (figure 5), with a major peak at 17.3 eV, also marked by an arrow, and also in chromium ions (figure 6), with a marked peak at 17.6 eV. In the case of copper ions, the net-TR diagram is plotted here with a logarithmic ordinate scale (figure 7), and, besides the $Ne^+$-CT excited states slightly below 21.56 eV, a strong radiative de-excitation was observed for states around 22.2 eV. The positions of these peaks in the net-TR diagrams of $Fe^+$, $Mn^+$, $Cr^+$, $Cu^+$ ions follow a common pattern: they are ≈5.6–5.8 eV *below the second ionization energy of the respective element Me*. A possible explanation is that the excited Me II

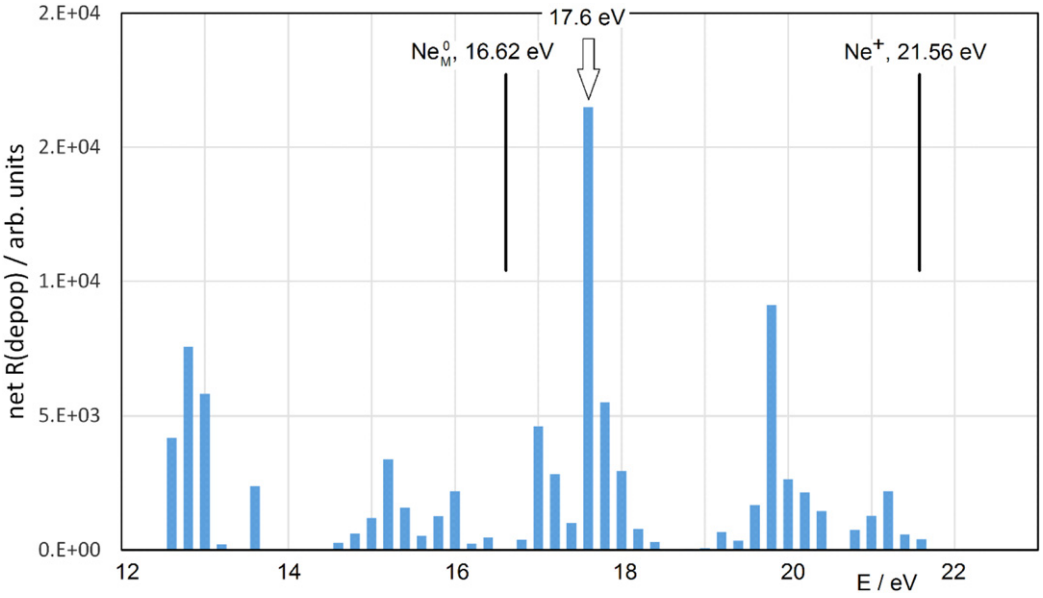


**Figure 6.** Net radiative depopulation rate of Cr II excited states as function of their energy in a neon GD.

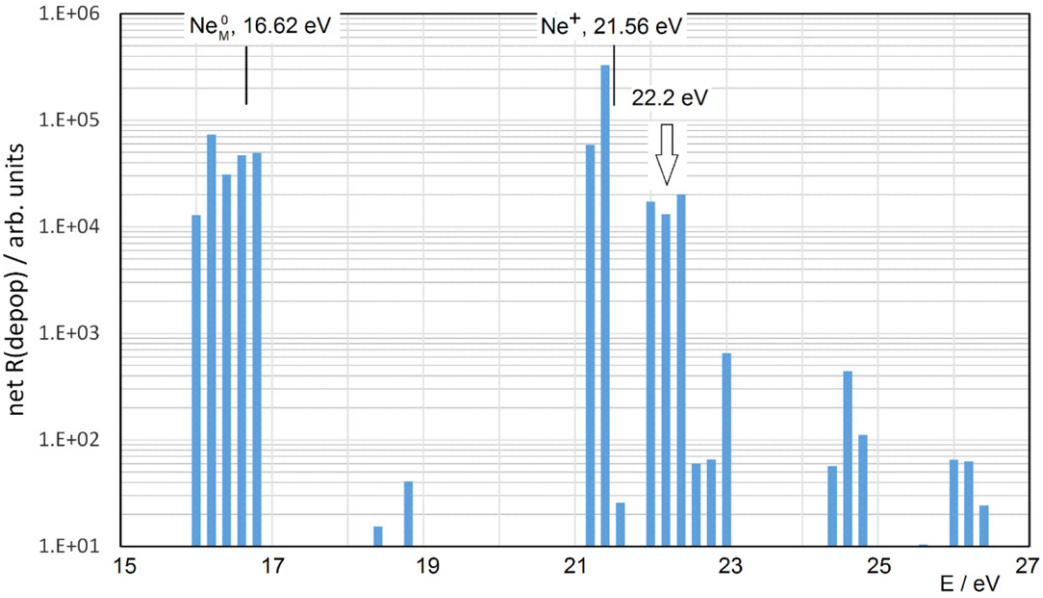


**Figure 7.** Net radiative depopulation rate of Cu II excited states as function of their energy in a neon GD.

states corresponding to these peaks can be populated by the following reaction[7]

$$Me^{++} + Ne^0{}_M \rightarrow Me^{+*} + Ne^+{}_0 + \Delta E, \qquad (7)$$

i.e., by a CT between doubly charged ions of the element Me and neutral neon metastables. In analogy with other CT processes, this reaction would be expected to have a resonance character, with a high cross section only in the vicinity of the resonance energy. There are two levels of the $Ne^+$ ions and four levels of $Ne^0{}_M$ metastables that can take part in the reaction (7), listed in table 2. Considering their energies and the energies of the $Me^+$ levels supposedly populated by this reaction (the peaks in the net-TR diagrams marked by arrows),

**Table 2.** Neon ions and neon neutral metastables that can take part in reaction (7) and their energies.

| $E$/eV | $Ne^+{}_0$ | $Ne^0{}_M$ |
|---|---|---|
| 21.56 | $2s^22p^5\ {}^2P^\circ_{3/2}$ | |
| 21.66 | $2s^22p^5\ {}^2P^\circ_{1/2}$ | |
| 16.62 | | $2s^22p^5(^2P^\circ_{3/2})3s\ {}^2[3/2]^\circ_2$ |
| 16.67 | | $2s^22p^5(^2P^\circ_{3/2})3s\ {}^2[3/2]^\circ_1$ |
| 16.72 | | $2s^22p^5(^2P^\circ_{1/2})3s\ {}^2[1/2]^\circ_0$ |
| 16.84 | | $2s^22p^5(^2P^\circ_{1/2})3s\ {}^2[1/2]^\circ_1$ |

[7] Symbols $Ne^0{}_M$ $Ne^+{}_0$ denote the states as listed in table 2. Although the $2s^22p^5\ {}^2P^\circ_{1/2}$ state of $Ne^+$ ion at 21.66 eV is metastable, it belongs to the $Ne^+$ ground term and as such it is listed here with the subscript 0, not M.

**Table 3.** Energies of the species participating in reaction (7) and other relevant parameters of this reaction.[a]

| | | | | Peak in the Me II net TR diagram | | | |
|---|---|---|---|---|---|---|---|
| Element | $E(Me^{+}{}_0)$ eV | $Me^{++}{}_0$ | $E(Me^{++}{}_0)$ eV | $E$(peak) eV | $2S+1$ | $E(Me^{++}{}_0) - E$(peak) eV | $\Delta E$ in equation (7) eV |
| Fe | 7.90 | $3d^6\,{}^5D_4$ | 24.10 | 18.50 | 4 | 5.60 | 0.56–0.89 |
| Cr | 6.77 | $3d^4\,{}^5D_0$ | 23.26 | 17.67 | 6 | 5.59 | 0.55–0.88 |
| Mn | 7.43 | $3d^5\,{}^6S_{5/2}$ | 23.07 | 17.30 | 7 | 5.77 | 0.73–1.06 |
| Ti | 6.83 | $3d^2\,{}^3F_2$ | 20.40 | 14.58 | 4 | 5.82 | 0.78–1.11 |
| Cu | 7.73 | $3d^9\,{}^2D_{5/2}$ | 28.02 | 22.0–22.4 | 1, 3 | 5.62–6.02 | $>\approx$0.58 |

[a] $Me^{+}{}_0$ and $Me^{++}{}_0$ denote the ground state of the singly and doubly charged Me ions, respectively.

the energy defect $\Delta$E observed for this reaction would be $\approx$ 0.6–1.0 eV, see table 3. Also presented in table 3 are the energies of the species involved in reaction (7) and other relevant parameters. In column 6 of table 3 is the spin multiplicity of the states constituting the peaks marked by arrows in the net-TR diagrams. The Wigner spin rule applied to reaction (7) says that eligible levels of the product ion should have a multiplicity by 1 higher or lower than the multiplicity of the $Me^{++}$ ground state. Comparison of columns 3 and 6 in table 3 shows that the observed peaks comply with this.

In copper, the Cu II levels that can be excited by reaction (7) may also be populated by a CT reaction between metastable Cu atoms and $Ne^{+}$ ions [20]. This makes the reasoning about whether or not, or to which extent reaction (7) contributes to the population of those Cu II levels, somewhat uncertain. In Ti, the situation is different from the other elements listed in table 3: the second ionization energy of Ti (20.40 eV) is lower than the energy of $Ne^{+}$ ions, and, therefore, the $Ne^{+}$–$Ti^0$ CT reaction leads to the creation of $Ti^{++}$ ions (charge transfer and ionization, CTI [21]). A major population mechanism of the $Ti^{+*}$ excited ions in the plasma is then the reaction

$$Ti^{++} + Ti^{0}{}_0 \rightarrow Ti^{+}{}_0 + Ti^{+*}. \qquad (8)$$

This process is responsible for the emission from the Ti II states around 13.4 eV [13], see figure 8. The subscript '$_0$' in equation (8) indicates the ground state, to distinguish it from an excited state, indicated by an asterisk. The energy peak in the net TR diagram corresponding to reaction (7) with $\Delta E = 0.8$ eV for titanium is 14.6 eV, see the arrow in figure 8. There is significant emission from Ti II states in the vicinity of that energy. This is, however, below the energy of neon metastables (16.62 eV). Hence, PI of neutral titanium by neon metastables may play a role also and is probably responsible for the Ti II emission from levels between 15 and 16.5 eV. In the bottom of figure 8 is a schematic diagram of all existing Ti II levels, sorted according to their spin multiplicity and energy. This shows that the electronic structure of the species under study may of course significantly affect the observed pattern of the net radiative depopulation rate.

The existence of doubly charged ions in a neon GD was confirmed by emission spectroscopy for titanium [13] and zinc[8], always by few weak Me III lines. Much more persuasive results in this respect were obtained by mass spectrometry [21]. $Me^{++}$ ions can be created by energetic collisions in the cathode sheath and also by PI by neon metastables of $Me^{+}$ ions, in the negative glow region. The latter process appears to be primarily responsible for the effects reported here, as they were observed in a neon discharge only, not argon. This can be explained by the difference in the energy of argon and neon metastables (11.55 eV, 16.62 eV, respectively): unlike neon, argon metastables do not have enough energy to further ionize $Me^{+}$ ions of the elements mentioned. For copper, this applies to $Ne^{0}{}_M$ metastables also. But, as already mentioned, the peak in the Cu II net TR diagram corresponding to reaction (7) coincides with the emission caused by the ($Cu^{0}{}_M$–$Ne^{+}$) CT reaction. It is thus unclear whether the reaction (7) with Me = Cu takes place.

The energy defect $\Delta E$ of reaction (7) was found to be higher than that of CT reactions of the type (4) and (5) for all the elements studied. This may be associated with the difference in the charge states of the reacting species: in reaction (7), the Debye sphere around a doubly charged ion, $Me^{++}$, changes itself into two Debye spheres around singly charged ions $Ne^{+}$, $Me^{+}$, whilst in reactions (4) and (5), there is only a change of the positive ion inside an already existing Debye sphere. The energy difference associated with these processes may be the reason for the higher observed energy defect $\Delta E$ in reaction (7) than (4) and (5).

The presence of $Me^{++}$ ions logically raises the question of whether the process analogous to that represented by equation (8), i.e., the ($Me^{++}$–$Me^0$) CT reaction, takes place also for other elements than titanium. By considering which Me II levels can be populated by reaction (8) and comparing with the Me II net-TR diagrams presented above, the following conclusions can be drawn:

(a) There is an emission from Cr II, Mn II and Fe II levels that can be populated by the ($Me^{++}$–$Me^0$) CT reactions. But,
(b) For Mn, Cr, Fe the maximum energy of the $Me^{+}$ ions to be created by the ($Me^{++}$–$Me^0$) CT reaction is lower than the energy of neon metastables. Hence, it would be difficult to distinguish the Me II emission caused by ($Me^{++}$–$Me^0$) CT from that caused by PI by $Ne^{0}{}_M$ metastables of $Me^0$ atoms.
(c) For copper: there are no Cu II levels in the vicinity of the maximum energy of $Cu^{+}$ ions that could be

[8] Zn III lines at 162.251 nm, 162.919 nm, 163.933 nm, 164.482 nm and 167.305 nm (unpublished data).

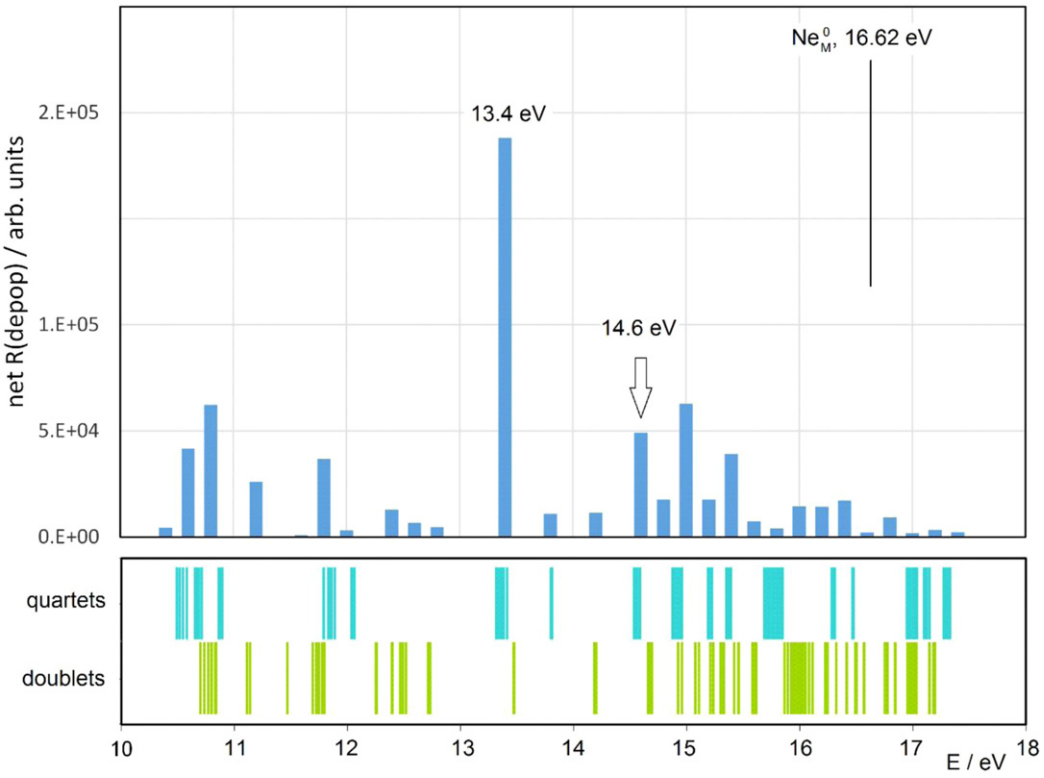


**Figure 8.** Net radiative depopulation rate of Ti II excited states as function of their energy in a neon GD. In the bottom is the distribution of all Ti II states in the given energy range, sorted by their spin multiplicity.

eventually created by the ($Cu^{++}$–$Cu^0$) CT process. Hence, logically, no emission was observed that would indicate this reaction could take place.

## 4. Uncertainty considerations

The evidence presented above should be discussed also from the point of view of the uncertainty associated with the data and possible sources of errors relevant for TR and net-TR formalism. The goal of this section is to identify major sources of the uncertainty and give some uncertainty estimates relevant to the conclusions of this study. Principal data in this study were relative intensities of individual lines in Me II emission spectra. In FT spectrometry, the noise associated with all lines within the spectral region recorded is distributed evenly[9] throughout that spectral region [40]. The strategy of the measurements must reflect this and a trade-off is needed between the spectral range collected, the requested spectral resolution and the duration of the experiment (the number of repetitive scans, known as co-adds. Co-addition improves SNR[10]). The FTS measurements were made in three overlapping spectral regions and the resulting linelists were subsequently combined. The details of the FTS measurements are in the papers dealing with individual elements, see the references in table 1. The spectra were radiometrically calibrated using standard lamps (a tungsten halogen lamp and a deuterium lamp) and the calibration was checked by the branching ratio method [6]. The uncertainties of relative intensities of the spectral lines then comprise the uncertainty in the radiometric calibration and also the uncertainty arising from the fit of the line and measurement of its intensity, which is 1/SNR in percentage, i.e. a line with SNR = 100 will have an uncertainty in its measured intensity of approximately 1%. For TR diagrams, all lines with SNR $>10$ were considered. Estimated combined relative uncertainty of the intensities of the weakest lines was ≈20%. For strong lines, the uncertainty was limited largely by radiometric calibration. A conservative estimate of its uncertainty, based on branching ratios, was ≈15% at maximum.

An advantage of the formalism of TR diagrams is that it depends solely on the measured spectrum, with no additional parameters required, because the rate $R_{ij}$ of a transition associated with a certain spectral line, $R_{ij} \sim (\lambda_{ij} I_{ij})$, depends solely on directly measured quantities: its wavelength $\lambda_{ij}$ and its intensity $I_{ij}$. This is in contrast to a more common formalism of Boltzmann plots [6] in which it is frequently the availability and the accuracy of the relevant transition probabilities $A_{ik}$ what limits the uncertainties associated with individual points and the Boltzmann plot as a whole [38].

There are two major points to be considered in connection with a TR diagram: its completeness and its meaning (physical context). The former point means the following: the spectral range recorded (in this study, $\lambda_{ij} \approx 160$–$600$ nm) defines which

[9] This applies if intensity (spectral density) in the spectrum is expressed with equidistant steps in wavenumber, not wavelength.
[10] SNR = signal-to-noise ratio.

transitions are included. Here it was the transitions for which $\Delta E_{ij} = 2.07$ to 7.74 eV. This range is sufficient to describe well the processes discussed in the previous section, as all major transitions by which the selectively excited Me II levels decay are within this range. Another question is whether *all existing decay paths* from those levels are included in the TR diagram under study. This is not always the case, in particular the highest excited levels must be considered with caution. As an example, some Fe II levels around 21 eV, excited by the ($Fe^0$–$Ne^+$) CT reaction, decay also directly into low-lying Fe II terms ($a^6D$ and $a^4D$), with $\lambda_{ij} \approx 93$–105 nm [19, 26], besides the cascade observed and shown in the TR diagram in figure 3.

TR diagrams such as those in figures 2 and 3 are not substantially affected by the uncertainty associated with the experimental data, as they are plotted with a logarithmic ordinate scale, and, in this format, confidence intervals of individual points ($\leqslant$10%–20%) would be comparable with the size of the corresponding symbols in the plots. In net-TR diagrams, figures 4–6 and 8, ordinate scale is linear. However, by grouping the points (the excited levels involved) into the 0.2 eV-wide intervals, each column in those diagrams represents several (many) levels and relative uncertainty of the combined quantity (the height of the column) decreases as $1/\sqrt{n}$ where $n$ is the number of the levels involved. This uncertainty is then negligible compared to the features observed (the peaks indicating selective excitation).

The last issue concerns the information contained in TR diagrams and its interpretation. The idea is that, under the approximation of radiatively-dominated deexcitation, collisional processes responsible for the population of certain excited levels manifest themselves by radiative decay of those levels. An ideal situation, in which virtually all the transitions are accurately reflected by a TR diagram, would be if radiative depopulation rates of excited levels substantially exceeded their depopulation rates by collisions with electrons:

$$n_i \sum_k A_{ik} \gg n_e n_i \sum_k \langle v\sigma \rangle_{ik} \tag{9}$$

where $n_i$ is the population of a level $i$, $n_e$ is the electron number density, $k$ denotes a lower level than $i$ and $\langle v\sigma \rangle_{ik}$ is the rate coefficient for the transition $i \rightarrow k$ caused by collisions with electrons. The rate coefficient $\langle v\sigma \rangle_{ik}$ can be expressed as

$$\langle v\sigma \rangle_{ik} = \int_0^\infty v \cdot \sigma_{ik}(E) \cdot f(v)\, \mathrm{d}v \tag{10}$$

where $v$ is the electron velocity, $f(v)$ is the electron velocity distribution function and $\sigma_{ik}(E)$ is the cross section of electron impact deexcitation. The processes of EI excitation and deexcitation are closely related, and, from the principle of microscopic reversibility, the following relation results for their cross sections $\sigma_{ik}$, $\sigma_{ki}$ [6]:

$$\sigma_{ik}(E) = \frac{g_k}{g_i} \frac{E + \Delta E}{E} \sigma_{ki}(E + \Delta E) \tag{11}$$

Here, $\Delta E = E_i - E_k$ and $g_i$, $g_k$ are the respective statistical weights (degeneracy factors) of the levels involved. Equation (11) says that EI deexcitation cross sections ($i \rightarrow k$, $\sigma_{ik}$) and the corresponding EI excitation cross sections ($k \rightarrow i$, $\sigma_{ki}$) are comparable, whilst a provision is made for the fact that, in case of excitation, the corresponding energy must be higher by the excitation threshold, $\Delta E = E_i - E_k$. Excitation cross sections were published for $Cu^+$ and $Fe^+$ ions [33, 41], their values are in the order of $10^{-18}$ to $10^{-15}$ $cm^2$ and $10^{-18}$ to $10^{-17}$ $cm^2$, respectively. Taking $10^{-17}$ $cm^2$ as a typical cross section of EI deexcitation of excited $Me^+$ ions and considering typical parameters of a Grimm-type GD, $n_e = 2 \times 10^{14}$ $cm^{-3}$ and $T_e = 0.45$ eV [31, 32], a typical EI deexcitation rate, i.e. the right side of equation (9), will be $\approx n_i^*(2.5 \times 10^6\ s^{-1})$. With typical transition probabilities $A_{ik}$ of strong emission lines in the order of $10^7$ to $10^9$ $s^{-1}$, this suggests that equation (9) holds for most transitions observed. For completeness, a remark should be made about prospective deexcitation by heavy particle collisions. From kinetic theory of gases, it follows that a typical collision rate between heavy particles in a Grimm-type GD is $\approx n^* 10^8$ $s^{-1}$, which is comparable with the figure on the left side of equation (9). However, elastic collisions are irrelevant here and inelastic collisions with ground state Ne atoms (the $Me^{+*}$–$Ne^0$ Penning reaction) cannot affect the $Me^+$ levels discussed in section 3 (table 3, column 5) because of a large gap between the $Ne^0$ ground state and the first excited state (16.62 eV). Inelastic collisions with $Ne^0{}_M$ metastables are by orders of magnitude less frequent [43] and cannot thus violate the validity of equation (9) either.

Another sign that radiatively-dominated deexcitation is a good approximation for a Grimm-type GD is that in cascade excitation/deexcitation processes like that shown in figure 3, there are no levels for which a negative TR balance would arise, i.e. the situation in which the observed radiative population rate would significantly[11] exceed the observed radiative depopulation rate. If an intermediate level of such a cascade is not subject to additional collisional excitation, prospective significant EI depopulation would demonstrate itself by a negative radiative TR balance of that level.

## 5. A broader context: the character of glow discharge excitation and some other plasma processes considered

The processes described in previous sections may seem uncommon from the perspective of optical diagnostics of close-to-LTE plasmas, more frequently discussed than glow discharges. Therefore it is desirable to emphasize the differences and clarify some questions raised in this context, such as e.g. what the role of EI excitation is and why the spectra of doubly charged ions (Me III) are not mentioned if $Me^{++}$ ions are claimed to be responsible for the effects observed.

The first fact to realize is that, in optical spectroscopy, we can see only emission from non-metastable excited atoms or ions. Therefore the character of the emission spectrum depends (1) on the electron structure of the atom or ion under study, i.e., the availability and energy distribution of the levels from

[11] Beyond the measurement uncertainty.

which emission can occur, and (2) on the excitation conditions in the plasma, i.e., the population rates of eligible atomic/ionic levels mentioned under point (1). In context of the results presented above, it is reasonable to look more closely at doubly charged iron ions. The lowest non-metastable Fe III level has energy of 11.05 eV above the Fe III ground level [19]. Radiative transitions from lower Fe III levels, below 11.05 eV, are parity-forbidden, hence, to see the Fe III spectrum, Fe III levels with $E \geqslant 11.05$ eV would have to be sufficiently populated. Basic parameters controlling EI excitation are electron temperature $T_e$ and electron number density $n_e$ in the plasma. In a Grimm-type GD, $T_e \approx 0.45$ eV [31] and $n_e \approx 2 \times 10^{14}$ cm$^{-3}$ [31, 32]. The rate constant $k_E$ for the excitation of a level with energy $E_i$ by electrons with a temperature $kT_e$ is [6]

$$k_E = \langle \sigma v \rangle = \int v\sigma(v) f(v)\,\mathrm{d}v = \int_{E_i}^{\infty} \sqrt{\frac{2E}{m_e}}\sigma(E) \sqrt{\frac{E}{\pi}} \frac{2}{(kT_e)^{3/2}} e^{-\frac{E}{kT_e}}\,\mathrm{d}E \qquad (12)$$

where $f(v)$ is the Maxwellian velocity distribution of the electrons and $\sigma(v)$, $\sigma(E)$ is the excitation cross section of that level, whilst the electrons are characterized either by their velocity $v$ or energy $E$. The cross section $\sigma(E)$ rises sharply from zero at the excitation threshold, $E_i$, to typical values $\leqslant 10^{-15}$ cm$^{-2}$ and then slowly decreases at higher electron energies [33]. Due to the exponential term in equation (12), EI excitation becomes negligible for higher $E_i/kT_e$ ratios, and, based on an analogy with EI excitation of neutral iron in the same discharge [26], it follows that the expected emission intensities from a level with $E_i = 11$ eV, if populated by EI excitation, would be at least by 4 orders of magnitude weaker than the weakest lines detectable in the experimental setup used[12]. This is why no Fe III emission was observed. A similar situation exists in manganese: the lowest non-metastable Mn III level has an even higher energy, 13.64 eV above the Mn III ground level [19]. The existence of $Me^{++}$ ions in neon and argon GD-s was confirmed by mass spectrometry [21, 42] [13]. The most likely source of $Me^{++}$ ions of the elements mentioned here, in the negative glow region, is the Penning ionization of $Me^+$ ions by $Ne^0{}_M$ metastables:

$$Me^+ + Ne^0{}_M \rightarrow Me^{++} + Ne^0{}_0 + e^- + \Delta E \qquad (13)$$

In the case of iron, the excess energy is $\Delta E \approx 0.5$ eV, in the case of manganese it is ≈1.05 eV. This energy is carried away by the electron released. The first excited level in the Fe III system has energy of 2.41 eV above the Fe III ground level [19], hence, this process can create only ground state $Fe^{++}$ ions. Likewise in manganese: the first excited level in Mn III has energy of 3.33 eV.

The approach adopted in this study was to consider all potentially relevant processes, identify those that can dominate the excitation of the Me II levels with high net radiative depopulation rates and show which processes are marginal in this respect and why. EI excitation of ground-state or metastable $Me^+$ ions cannot explain the effects described here because of a high energy of the Me II levels from which emission was observed (see table 3, equation (12) and the explanation in the previous paragraph concerning EI excitation of $Me^{++}$ ions). Other potentially relevant processes involving electrons is radiative and dielectronic (3-body) recombination of $Me^{++}$ ions (RR and DR, respectively). In the former case (radiative capture of an electron), the highest cross-section occurs if the resulting $Me^+$ ion is in the ground state. Cross-sections of RR with final $Me^+$ ions in various excited states monotonically decrease with their energy [34]. This pattern does not correspond to the Me II net depopulation rates observed[14]. DR preferentially populates the highest excited levels of the resulting atom or ion [33], and, together with EI ionization, DR is believed to be largely responsible for a strong coupling in partial-LTE plasmas between the continuum (free electrons) and the highest bound electron levels [35]. An advanced treatment of EI excitation, DR and RR processes can be found in [36]. As a conclusion of this paragraph, no indication was found in the literature that EI processes could possibly explain the selective population of the Me II levels observed. Therefore other mechanisms than electron collisions must be considered, i.e., those involving heavy particles. Heavy particle collisions play generally an important role in rare gas-diluted plasmas such as GDs. This can be illustrated on the following example: in an argon GD with Fe cathode, the ($Ar^+$–$Fe^0$) ACT reaction, selectively populating Fe II levels in a narrow energy interval between 15.3 and 16.1 eV, is responsible for 75% of the total Fe II emission[15] (see also figure 3). That is more than the total Fe I emission from that discharge (44% of Fe II emission) [26]. The rate constant of this reaction is $k_{ACT}(Ar^+–Fe^0) \approx (7.6 \pm 3.0) \times 10^{-9}$ cm$^3$ s$^{-1}$ [37]. This is in compliance with the results of Bogaerts and Gijbels [39], who calculated by Monte Carlo simulation the complete electron energy distribution function (EEDF) for a discharge like this and showed that EI ionization can be neglected, in contrast to other processes like CT or PI reactions.

Another point worth mentioning here is the methodology used. It was shown many times that common methods of optical plasma diagnostics which are based on Saha–Boltzmann statistics generally do not work for glow discharges. An alternative is the formalism of TR diagrams that is very successful

[12] Here, a very conservative estimated upper limit of relative number density of doubly charged iron ions was used: $n(Fe^{++})/n(Fe^0) < 0.1$. GD is a non-equilibrium plasma, hence, this ratio cannot be estimated by the Saha equation. In a Grimm-type GD with a copper cathode, the $n(Cu^{++})/n(Cu^0)$ ratio, calculated by computer simulations, was reported to be as low as ≈$10^{-4}$ [33].

[13] In reference [21], it was reported that the $Me^{++}/Me^+$ signal ratios are greater by a factor of ≈$10^2$ in a Ne discharge than Ar for Fe, Cu and by a factor of ≈$5 \times 10^2$ for Ti, in a 'fast-flow' GD source for mass spectrometry. That is also a flat cathode GD source, with a similar geometry like the source used in this study, and operated at similar macroscopic discharge conditions (voltage, current density at the cathode and the working gas pressure).

[14] Exact RR cross sections were reported in [34] for hydrogen, i.e. the $H^+ + e^- \rightarrow H^{0*}$ reaction, and a plausible explanation is given there why heavier ions should follow a similar pattern. RR cross sections are small, in the order of $10^{-20}$ cm$^2$ [34]. This is why no characteristic 'recombination spectra' (a continuous spectrum with sharp edges at the binding energy of the levels) were observed and why RR is a marginal process in this plasma.

[15] In terms of transition rates, i.e. photons per second.

in the interpretation of Me II spectra from Grimm-type GDs for which the approximation of radiatively-dominated depopulation holds. TR diagrams is the method of choice if there is a need to correct for cascade excitation by radiative decay of higher excited levels and identify selective excitation- and ionization processes. The use of TR diagrams, however, has its costs: to establish a reasonably complete TR diagram, a high-resolution intensity-calibrated emission spectrum is needed, covering a wide and continuous wavelength range, typically from vacuum UV to the visible region. This is a very demanding requirement that can be fulfilled at present only by a high-resolution visible-VUV FTS spectrometer. There are only few such instruments worldwide. A GD emission spectrum of a transition element typically consists of many hundreds or thousands of lines and their correct identification and subsequent data processing is also a demanding task.

## 6. Conclusions

Emission spectra of singly charged ions of transition elements in a Grimm-type glow discharge are dominated by transitions from levels excited largely by various second-kind heavy particle collisions with the ions and metastable atoms of the discharge gas. A powerful method of studying such excitation mechanisms in this type of plasma is a systematic analysis of its emission spectrum, based on the recently introduced formalism of transition rate (TR) diagrams, in which relative rates of radiative population/depopulation of individual levels of the atom or ion under study are plotted as functions of their energy. The rates corresponding to cascade excitation (radiative decay of higher excited states) can be subtracted and the resulting net TR diagrams reflect the population of individual levels by collisional processes. TR diagrams are most useful in plasmas in which radiative decay of excited states dominates over their depopulation by collisions with electrons.

Important ionization/excitation mechanisms in glow discharge plasmas are charge transfer processes, e.g. asymmetric charge transfer between ions of the discharge gas and atoms of various elements sputtered from the cathode. These reactions have a resonance character and can be identified by a peak at the resonance energy in the TR diagram of a species produced by the reaction. The resonance energy is characteristic for each reacting pair. For all elements listed here, the ($Ne^+$–$Me^0$) charge transfer reaction is a major ionization mechanism of the element Me in a neon glow discharge plasma.

By using the net TR diagram method, it was found that the spectra of singly charged ions of Fe, Ti, Cr, Mn in a glow discharge in neon exhibit strong emission from levels populated by charge transfer reactions between doubly charged ions of the respective element and neutral neon metastables. A detailed analysis suggests that no other process can explain the selective nature of the Me II emission with the pattern observed. To our knowledge, it is the first time this mechanism is reported. It contributes significantly to the creation of excited ions of these elements and should be included in collisional-radiative models of neon GD plasmas. Comparison with an argon discharge suggests that the doubly charged ions of these elements in a neon plasma are created largely by Penning ionization by neon metastables of singly charged ions of the respective element. In the case of titanium, the $Ti^{++}$ ions are created also by charge transfer and ionization, in collisions between neutral titanium atoms and neon ions.

From a broader perspective, it should be stressed that, in glow discharges, various second-kind heavy particle collisions are a major source of excited ions of the elements sputtered from the cathode and very likely a major source of the ionization of these elements as a whole. Consequently, they should no longer be considered as mere perturbations, causing deviations from otherwise close-to-LTE conditions in the plasma, but as principal ionization paths. A relevant description of such plasmas will then be by collisional-radiative models in which such processes would play a key role, rather than the Saha–Boltzmann distribution and deviations therefrom. A caution in this respect is also desirable in the interpretation of emission spectra of other laboratory plasmas.

## Acknowledgments

The spectral data from the high resolution VUV-VIS Fourier transform spectrometer at Imperial College, London, UK, were collected during author's visit to IC in 2010, financially supported under the GLADNET Analytical Glow Discharge Network within the 6th Framework Program of the EU, contract Nr MRTN-CT-2006-035459. The subsequent work was supported by the Operational Program 'Research, Development and Education' financed by European Structural and Investment Funds and the Czech Ministry of Education, Youth and Sports (Project No. SOLID21 - CZ.02.1.01/0.0/0.0/16_019/0000760).

## ORCID iDs

Zdeněk Weiss https://orcid.org/0000-0001-7364-1325

## References

[1] Bings N H, Bogaerts A and Broekaert J A C 2010 Atomic Spectroscopy: A Review *Anal. Chem.* **82** 4653–81
[2] Sanz-Medel A, Pereiro R and Costa-Fernandez J 2009 *A General Overview of Atomic Spectrometric Techniques, RSC Analytical Spectroscopy Series Monographs no 10* ed J M Andrade-Garda (Cambridge: Royal Society for Chemistry)
[3] Britun N, Minea T, Konstantinidis S and Snyders R 2014 Plasma diagnostics for understanding the plasma–surface interaction in HiPIMS discharges: a review *J. Phys. D: Appl. Phys.* **47** 224001
[4] Sneden C, Lawler J E and Wood M P 2018 Application of laboratory atomic physics to some significant stellar chemical composition questions *Atoms* **6** 48
[5] Little C E 1999 *Metal Vapor Lasers* (Chichester: Wiley)
[6] Thorne A, Litzén U and Johansson S 1999 *Spectrophysics: Principles and Applications* (Berlin: Springer)
[7] Cristoforetti G, De Giacomo A, Dell' Aglio M, Legnaioli S, Tognoni E, Paleschi V and Omenetto N 2009 Local thermodynamic equilibrium in laser-induced breakdown spectroscopy: beyond the McWhirter criterion *Spectrochim. Acta* B **65** 86–95

[8] Turner-Smith A R, Green J M and Webb C E 1973 Charge transfer into excited states in thermal energy collisions *J. Phys. B: Atom. Molec. Phys.* **6** 114–30
[9] Duffendack O S and Black J G 1929 Studies on the spectra of Cu I, Cu II and Mn II by means of a vacuum tungsten furnace *Phys. Rev.* **34** 35
[10] Steers E B M and Fielding R J 1987 Charge transfer excitation processes in the Grimm lamp *J. Anal. Atom. Spectrom.* **2** 239–44
[11] Weiss Z, Pickering J C and Hoffmann V 2019 Sixty years of spectroscopic research: a tribute to Professor Edward B M Steers *Chem. Papers* **73** 2891–6
[12] Weiss Z, Steers E B M and Pickering J C 2015 Transition rates and transition rate diagrams in atomic emission spectroscopy: a review *Spectrochim. Acta B* **110** 79–90
[13] Weiss Z, Steers E B M and Pickering J C 2018 Transition rate diagrams and excitation of titanium in a glow discharge in argon and neon *Spectrochim. Acta* B **144** 20–8
[14] Weiss Z, Steers E B M, Pickering J C and Mushtaq S 2014 Excitation and transition rate diagrams of singly ionized iron in analytical glow discharges in argon, neon and an argon–hydrogen mixture *J. Anal. At. Spectrom.* **29** 2078–90
[15] Marcus K R and Broekaert J A C 2003 *Glow Discharge Plasmas in Analytical Spectroscopy* (Chichester: Wiley)
[16] Nelis T and Payling R 2003 *Glow Discharge Optical Emission Spectroscopy: A Practical Guide, RSC Analytical Spectroscopy Monographs* (Cambridge: The Royal Society for Chemistry)
[17] Pickering J C 2002 High resolution Fourier transform spectroscopy with the Imperial College (IC) UV-FT spectrometer, and its applications to astrophysics and atmospheric physics: a review *Vib. Spectrosc.* **29** 27
[18] Weiss Z, Steers E B M, Pickering J C and Mushtaq S 2014 Transition rate diagrams—a new approach to the study of selective excitation processes: the spectrum of manganese in a Grimm-type glow discharge *Spectrochim. Acta, Part* B **92** 70–83
[19] Kramida A, Ralchenko Y and Reader J and NIST ASD Team 2018 *NIST Atomic Spectra Database* (*Version 5.6.1*) (Gaithersburg, MD: National Institute of Standards and Technology) https://physics.nist.gov/asd
[20] Weiss Z, Steers E B M, Pickering J C, Hoffmann V and Mushtaq S 2014 Excitation of higher levels of singly charged copper ions in argon and neon glow discharges *J. Anal. At. Spectrom.* **29** 2256–61
[21] Mushtaq S, Steers E B M, Barnhart D, Kasik M, Churchill G, Richter S, Pfeifer J and Putyera K 2017 The production of doubly charged sample ions by 'charge transfer and ionization' (CTI) in analytical GD-MS *J. Anal. At. Spectrom.* **32** 1721–9
[22] Gianfrani L, Monda O, Sasso A, Schisano M I, Tino G M and Inguscio M 1991 Visible and ultraviolet high resolution spectroscopy of Ti I and Ti II *Opt. Commun.* **83** 300–6
[23] Huldt S, Johansson S, Litzén U and Wyart J F 1982 The spectrum and term system of singly ionized titanium, Ti II *Phys. Scr.* **25** 401–12
[24] Pickering J C, Thorne A P and Perez R 2001 Oscillator strengths of transitions in Ti II in the visible and ultraviolet regions *Astrophys. J. Suppl. Ser.* **132** 403–9
[25] Kramida A and Sansonetti J E 2013 Energy levels and spectral lines of singly ionized manganese (Mn II) *Astrophys. J. Suppl. Ser.* **205** 14
[26] Weiss Z 2019 Excitation and ionization of iron in argon and neon glow discharges: towards the true picture *Spectrochim. Acta, Part* B **158** 105637
[27] Nave G and Johansson S 2013 The spectrum of Fe II *Astrophys. J. Suppl. Ser.* **204** 1
[28] Fuhr J R and Wiese W L 2006 A critical compilation of atomic transition probabilities for atomic and singly ionized iron *J. Phys. Chem. Ref. Data* **35** 1669
[29] Kramida A, Nave G and Reader J 2017 The Cu II spectrum *Atoms* **5** 9
[30] Sansonetti C J and Nave G 2014 Extended analysis of the spectrum of singly ionized chromium (Cr II) *Astrophys. J. Suppl. Ser.* **213** 28
[31] Bogaerts A, Quentmeier A, Jakubowski N and Gijbels R 1995 Plasma diagnostics of an analytical Grimm-type glow discharge in argon and in neon: Langmuir probe and optical emission measurements *Spectrochim. Acta* B **50** 1337–49
[32] Fang D and Marcus R K 1991 Effect of discharge conditions and cathode identity on charged particle populations in the negative glow region of a simple diode glow discharge *Spectrochim. Acta* B **46** 983–1000
[33] Bogaerts A, Gijbels R and Carman R J 1998 Collisional-radiative model for the sputtered copper atoms and ions in a direct current glow discharge *Spectrochim. Acta* B **53** 1679–703
[34] Massey H S W and Burhop E H S 1952 *Electronic and Ionic Impact Phenomena* (Oxford: Clarendon) pp 332–41
[35] van der Sijde B, van der Mullen J A M and Schram D G 1984 Collisional radiative models in plasmas *Beitr. Plasmaphys.* **24** 447–73
[36] Pradhan A K and Nahar S N 2011 *Atomic Astrophysics and Spectroscopy* (Cambridge: Cambridge University Press)
[37] Korolov I, Bánó G, Donkó Z, Derzsi A and Hartmann P 2011 Experimental study of the asymmetric charge transfer reaction between Ar+ ions and Fe atoms *J. Chem. Phys.* **134** 064308
[38] Weiss Z 2020 Glow discharge excitation and ionization of chromium, comparison with iron *Spectrochim. Acta* B **166** 105792
[39] Bogaerts A and Gijbels R 1996 Relative sensitivity factors in glow discharge mass spectrometry: the role of charge transfer ionization *J. Anal. At. Spectrom.* **11** 841–7
[40] Davis S P, Abrams M C and Brault J W 2001 *Fourier Transform Spectrometry* (New York, NY: Academic)
[41] Smirnov Y M 2000 Excitation of Fe I and Fe II in electron-atom collisions *Quantum Electron.* **30** 1019–24
[42] Hecq M and Hecq A 1984 Presence of douby-ionized metal ions in rare gas glow discharges *J. Appl. Phys.* **56** 872–3
[43] Bogaerts A and Gijbels R 1997 Comparison of argon and neon as discharge gases in a direct-current glow discharge: a mathematical simulation *Spectrochim. Acta* B **52** 553–65